How structural elements added in evolution from bacterial transporters serve human SLC6 homologs

Asghar M. Razavi[1], George Khelashvili[1], Harel Weinstein[1,2]*

[1]Department of Physiology and Biophysics, Weill Cornell Medical College of Cornell University, New York, NY, 10065, USA
[2]Institute for Computational Biomedicine, Weill Medical College of Cornell University, New York, NY 10065, USA

*Correspondence and requests for materials should be addressed to H.W. (haw2002@med.cornell.edu)

Abstract

Much of the structure-based mechanistic understandings of the function of neurotransmitter transporter family (SLC6A) proteins emerged from the study of their bacterial LeuT-fold homologs. It has become evident, however, that structural differences such as the long N- and C-termini of the eukaryotic neurotransmitter transporters are likely to impart phenotypic properties not shared by the bacterial homologs. These structural "additions" to the common molecular architecture have been shown to be involved in functions, including reverse transport (efflux), regulated by phosphorylation and by interactions with lipids found only in the eukaryotic cell membranes. To learn how the phenotypes of the eukaryotic transporters are enabled by molecular mechanisms involving these structural additions we have used large-scale molecular dynamics simulations of the wild type and mutant constructs of the human dopamine transporter (hDAT), and comparative Markov State Model analysis. The results reveal a rich spectrum of interactions of the hDAT N-terminus and distinguish different roles of the distal and proximal segments of the N-terminus, and interactions with the C-terminus, in modulating functional phenotypes not shared with the bacterial LeuT-like homologs.

Keywords: dopamine transport, SLC6 neurotransmitter transporters, evolutionary gain of function

Background

The dopamine transporter (DAT) is a member of the neurotransmitter:sodium symporter (NSS) family of proteins belonging to the solute carrier 6 (SLC6) family that performs the reuptake of dopamine from the synaptic cleft into the presynaptic nerve required for neuronal signaling (1). The essential role of DAT, and of its closely related homologs – the serotonin and norepinephrine transporters (SERT and NET) – in signal termination at the synapse makes them important targets for psychostimulants such as cocaine and amphetamines, as well as for pharmaceutical treatment of a variety of disorders of the nervous system (2). Moreover, genetic modifications of the functions of these transporters (3,4) have been implicated in diseases including Schizophrenia, Parkinson's, and Attention-deficit/hyperactivity disorder (ADHD). Reverse transport of the neurotransmitters (efflux) mediated by DAT and SERT, which has been shown to be affected by such disease-related mutations, is currently a very active topic of research on mechanisms of these membrane proteins (4-15).

Much has been learned about these mammalian neurotransmitter transporters from the investigation of structure and function of their bacterial homologs with which they share many structural and mechanistic properties (16-19). It has become clear, however, that one of the most important

structural differences between the eukaryotic and bacterial proteins, and in particular their much longer N- and C-termini that have been proposed to be partially structured (20,21), are involved in intricate mechanisms of their functional regulation. These structural differences are key to the functional phenotypes of the mammalian NSS that are not shared with the bacterial homologs (22-24). Such mechanisms involve various modes of interaction of the N- and C-termini with intracellular regions of the transporters, which in some cases are mediated or supported by specific components of the cell membrane as well as other proteins in the membrane or its vicinity (24-28). For example, the phosphorylation of the N-terminus has been shown to promote the efflux functions of the human DAT (hDAT) (22,26), and disruption of electrostatic interactions between the hDAT N-terminus and negatively charged PIP2 lipids in the membrane have been demonstrated to selectively impair the amphetamine (AMPH)-induced efflux (29), but not regular uptake.

While structure-based mechanistic details of these regulations of eukaryotic NSS function are still sparse, computational studies of hDAT have illuminated the role of the PIP2 lipid component of membranes in enabling the N-terminus of DAT to engage in functionally important interactions required to achieve conformational changes related to function(30), such as (i)-the transition of the DAT from outward-facing to inward-facing configurations (31), and (ii)-the release of the sodium ion from the Na2 binding site that is known to precede substrate transport and can serve as a probe to monitor the initial stages of the functional mechanism (32). Specifically, the PIP2-mediated N-terminus interactions with intracellular loop 4 (IL4) of hDAT was implicated in the facilitation of intracellular gate breaking (30), which leads to increased hydration of functionally important sites and to the release of Na^+ from the Na2 binding site to the intracellular environment (32). Since the release of Na^+ from the Na2 site is an important early step in the NSS transporter cycle (33,34), the interplay between N-terminus and PIP2 becomes involved in functional mechanisms of the transporter. This inference is even more interesting in light of experimental studies that have pointed to minimal involvement of PIP2 lipids in neurotransmitter uptake (35), while PIP2 is considered essential for efflux (29,36).

Reasoning that this intriguing difference in the role of PIP2 most likely reflects different roles of interaction of the N-terminus in the functional mechanism, we hypothesized that such roles may involve different modes of association with the membrane under various conditions (e.g., with/without PIP2) and for different hDAT constructs (e.g., phosphorylated or mutated N-terminus). Such different modes of N-terminus interaction with the membrane would then reorganize the positions, strengths, and dynamic consequences of its interaction with the other regions of the transporter. We undertook the present computational study of the role of the various interaction modes of the N-terminus in hDAT function to identify and understand their mechanistic details and consequences. Here we describe the results from extensive ensemble-level all-atom molecular dynamics simulations combined with Markov State Model analysis in the investigation of wild type hDAT dynamics modulated by mutated and/or modified N-terminus constructs and conditions. The results reveal preferred modes of interaction of the N-terminus with the intracellular domains of hDAT that can be associated with experimentally measured functional phenotypes of the transporter. We show how these interaction patterns can be altered under conditions that have been demonstrated to selectively affect efflux but not regular transport (e.g., PIP2 depletion, mutations such as R51W, K3A+K5A, or phosphomimic substitution, S/D, of Serine residues at positions 2, 4, 7, 12, and 13 (22,29,37) to Aspartate).

A rich spectrum of interactions of the rather long N-terminus of hDAT emerges from these studies, and the details of the molecular mechanisms can explain, for the first time, the different roles of the distal and proximal segments of the N-terminus in modulating specific functions of hDAT. It becomes clear how experimental manipulation of the N-terminus by partial truncation, mutations, and/or elimination of PIP2 interactions as described in the literature can have very different effects on uptake vs efflux functions of the transporter, further underscoring the central role played by this structural segment of the eukaryotic transporter that was added in the evolution from the bacterial LeuT-like members of this family.

Results

In a recent report (30) on the dynamics of PIP2-mediated interactions between specific regions of the N-terminus and IL4 region of hDAT, the N-terminus was shown to affect intracellular gate opening that leads to increased hydration of the substrate and ion binding sites from the intracellular side, culminating in the release of Na^+ ion from the Na2 site. The relation of the interactions observed in that system to functional mechanisms in hDAT prompted us to use extended ensemble MD computations (see Methods) to probe the dynamics of the hDAT N-terminus for constructs and conditions that impact the functional phenotypes, e.g., those demonstrated to selectively affect efflux. To this end, we accumulated and analyzed, as described in Methods, 50 statistically independent ~1 µs-long trajectories of (1) hDAT in PIP2-depleted membranes (hereafter referred to as "no-PIP2 system"), and (2) hDAT constructs with experimentally well-characterized mutations in the N-terminal domain including R51W, K3A+K5A (the "K3/5A system"), and the phosphomimic S/D construct in which first five N-terminal Ser residues are substituted by Asp, all of which were immersed in PIP2-containing bilayers.

To identify the regions of hDAT that interact with the N-terminus we generated the per-residue contact map shown in Figure 1. This map shows that with PIP2 present in the membrane, the N-terminus as a whole interacts with all intracellular loop (IL) regions of hDAT, i.e. IL1, IL2, IL3, IL4, and IL5, as well as with the C-terminus.

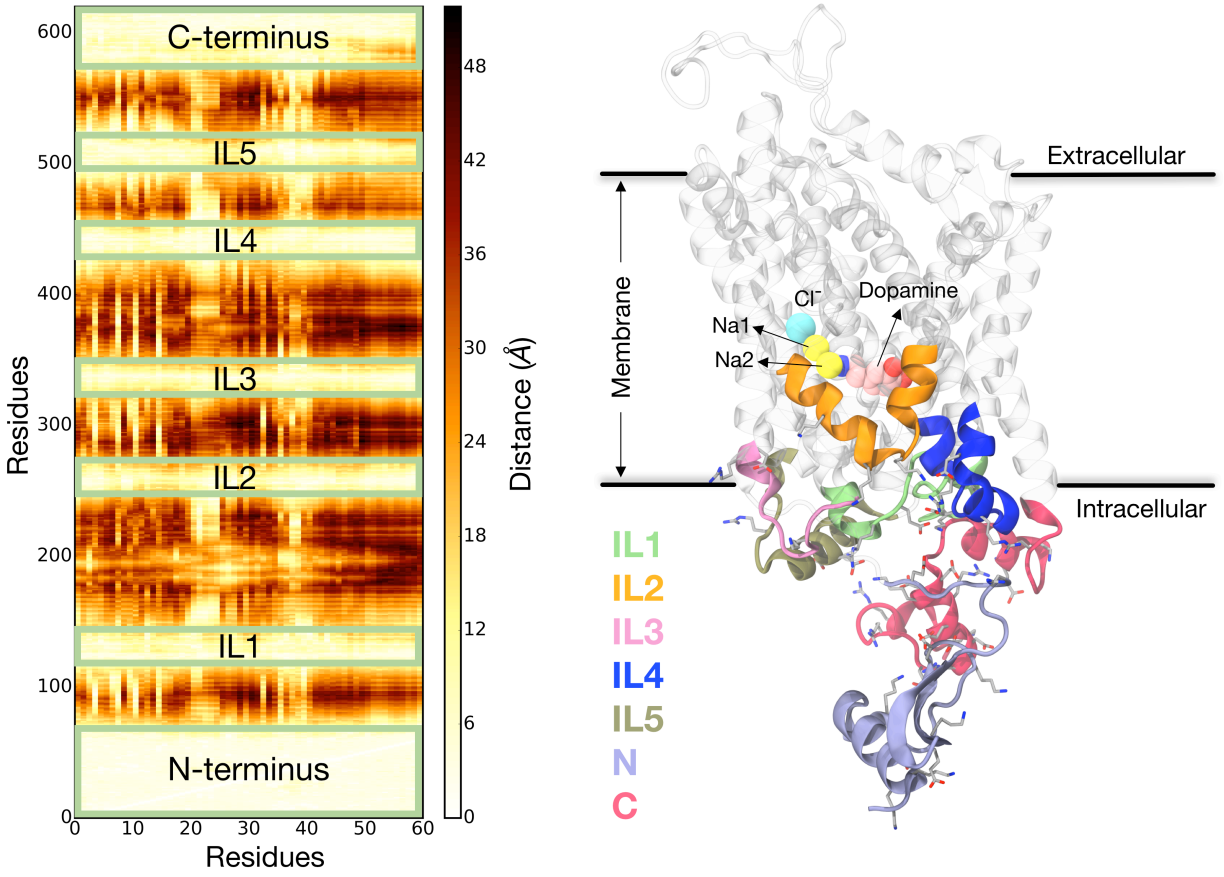

Figure 1. **hDAT structure and N-terminus interactions.** (**Left**) Contact map for interaction of N-terminus residues (x-axis) with all hDAT residues (y-axis). Distance calculations were done with the *closest-heavy algorithm* implemented in MDTraj software (38) . The color bar shows the minimum distance of each residue in the N-terminus to other residues (the lightest colored regions indicate the strongest interactions, e.g., in the various loop segments) as identified in the ensemble of 50 µs trajectories for the wild-type hDAT embedded in the PIP2-containing lipid bilayer (see Methods).

(**Right**) Snapshot of hDAT structure highlighting the intracellular segments interacting with the N-terminus in the ensemble of 50 μs trajectories. Charged residues are shown in licorice.

The correspondence between modes of interaction of the N-terminus and functional phenotypes of the dopamine transporter

A detailed analysis of the interactions between the N-terminus with the intracellular regions of hDAT in PIP2-containing and PIP2-depleted membranes reveals a specific pattern (modes) of interaction of the different parts of the terminus with intracellular regions of the transporter. Importantly, there is a remarkable correspondence between the detailed patterns of interactions and functional activity phenotypes determined experimentally for various constructs and conditions listed in Table 1. The modes of interaction of the N-terminus in the various constructs were quantified as the "interactions strength" (Figure 2) calculated as described in detail in Methods from the 50 × 1 μs trajectories accumulated for each construct and condition.

To account for experimental observations with a truncated N-terminus (ΔN22 system) that was shown to have distinct functional phenotypes both in DAT [21] and in SERT (35), we also split the calculation of the N-terminus modes of interactions into two groups: those of the *distal N-terminus* (residues 1 to 22), and of the *proximal N-terminus* (residues 23 to 57) (Figure 2). Results in Figure 2 clearly show that the N-terminus modes of interactions are different for the two groups across the different constructs. The difference between the groups is greatest for the interactions with IL1, IL4, and the C-terminus. The remarkable similarity between the pattern of interactions that the entire N-terminus makes with IL4 and the pattern of IL4 interaction with just the proximal part of the N-terminus (cf. circled regions in Figure 2) is especially noteworthy.

Table 1. Effects of various N-terminus constructs on hDAT uptake and efflux functions

Construct / Phenotype	Truncated N-terminus (ΔN22) (22)	K3A+K5A (K3/5A) (29)	PIP2 depleted membrane (no-PIP2) (29)	R51W (37)	S2D+S4D+S7D+S12D+S13D (S/D) (22)
Uptake	Not affected	Not affected	Not affected	Not affected	Not affected
Efflux	~80% reduced	~50% reduced	~80% reduced	~75% reduced	enhanced

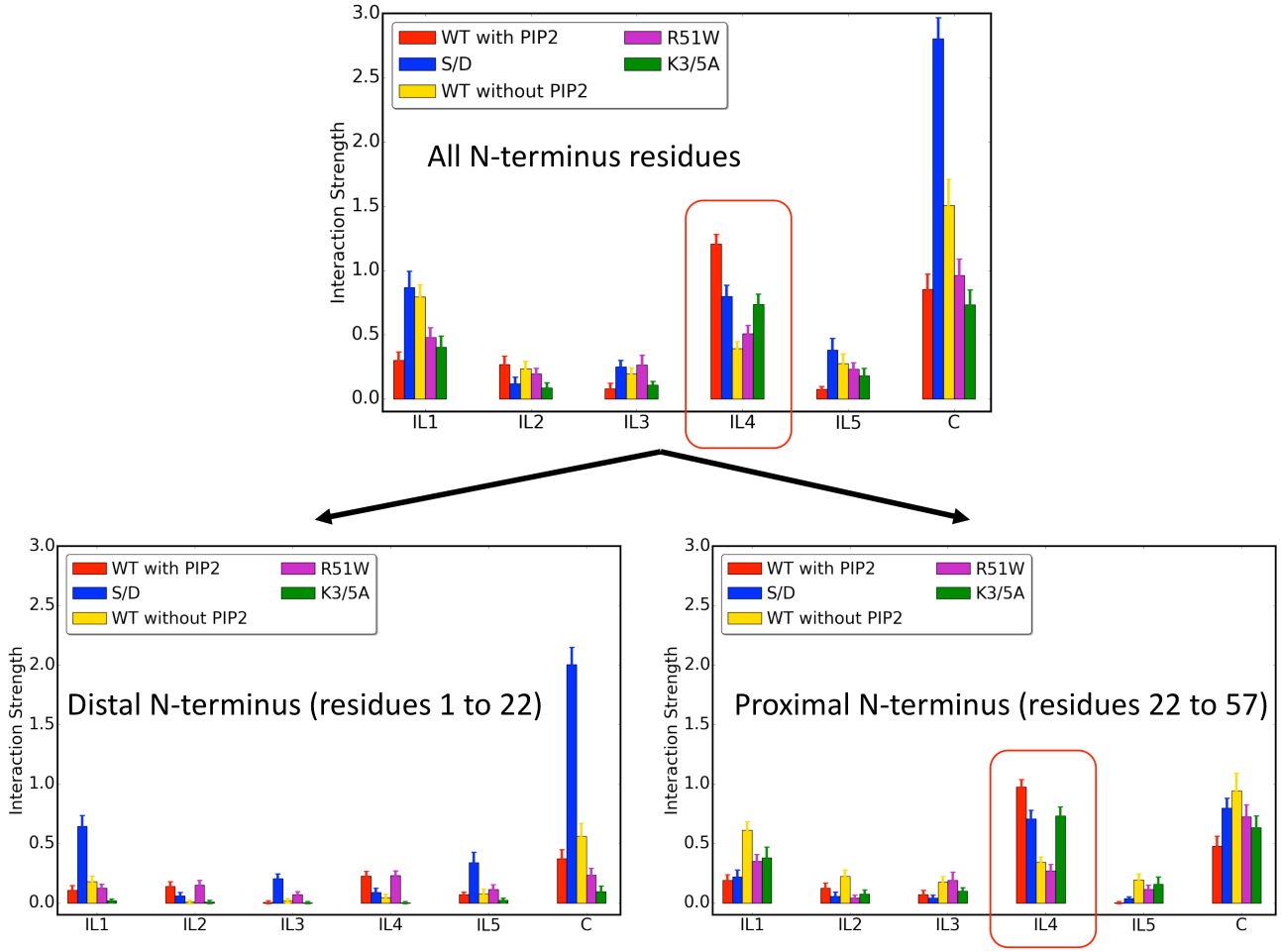

Figure 2. Modes of interaction of hDAT N-terminus with intracellular loop segments. The bars show the average interaction strength from all 50 trajectories of every construct, calculated as described in Methods, with error bars showing standard deviations calculated using the bootstrap method.

The functional role of the modes of interaction of the N-terminus with IL4 is underscored by their central role in the early steps of the substrate transport mechanism marked by Na^+ release from the Na2 site (30). Moreover, we showed (32) that the destabilization of the functional intracellular gates formed among residues R60, D436, R445, and E428 is required for the release process, and involves PIP2-mediated interactions between positively charged residues from N-terminus and positively charged residues from IL4. Consistent with these findings, Figure 2 shows that PIP2-mediated N-terminus/IL4 interactions observed in the wild type hDAT are disrupted upon PIP2 depletion or as a result of mutations that interfere with these interactions by eliminating contacts between the proximal part of the N-terminus (residue segment 23-57 that includes R51) and the IL4 region (residues 443-446, see Figure S1). The most stable interactions between gating residues E428–R445, as shown in Figure S2, are observed in the no-PIP2 system where we find the lowest count of the N-terminus/IL4 interactions (Figure 2).

Results in Figure 2 show that the distal N-terminus associates with the C-terminus in all the constructs we studied, but the degree of association varies between the systems. Indeed, for both the R51W and no-PIP2 systems the association between the distal N-terminus and the C-terminus is similar to that of the wild type (Figure 2). The weakest association with the C-terminus is observed for the K3/5A construct (in fact, the distal segment of this double mutant K3A/K5A N-terminus is seen to engage in the least amount of interactions with any of the intracellular loops), and the strongest

interaction with the C-terminus is in the S/D system. This diametrically opposed interaction characteristic of the two constructs relative to the wild type is intriguing, because only the S/D mutant construct has been shown to enhance dopamine efflux mediated by DAT, and in the absence of Amphetamine (AMPH) (22), while the K3/5A mutant, like several other constructs, produces a very low AMPH-induced efflux (29).

Mechanistic details of N-terminus involvement in the release of Na^+ from Na2

The release of Na^+ from the Na2 site, which initiates solute translocation by the hDAT, was shown to be directly related to the mode of interaction of the N-terminus with intracellular regions of the transporter with PIP2-containing membranes (32). Constructs differing in the modes of N-terminus interactions shown in Figure 2 also exhibit different probabilities of Na^+ release from the Na2 site on the same simulations scales. Spontaneous intracellular release occurred in 9/50 trajectories of the no-PIP2 system (Figure S3), in 3/50 trajectories of the R51W hDAT (Figure S4), and in a single trajectory of the S/D system (Figure S5). For comparison, in the similar time-scale ensemble MD simulations for WT hDAT in PIP2-containing membranes, release occurred in 12/50 trajectories (32). To understand the nature of the involvement of the N-terminus in the release mechanisms occurring in the different conditions and constructs, we analyzed the water penetration paths that open as a result of the modes of N-terminus interactions in each case.

Water penetration from the intracellular side of hDAT is a key step in the Na^+ release mechanism. In the wild type, the average correlation value between Na^+ release from the Na2 site, and the hydration of the Na2 site was found to be ~0.7 (32). Notably, this correlation was also observed in each trajectory in which Na^+ from Na2 site is released to the intracellular environment from the R51W, S/D, and no-PIP2 systems (Table S4), indicating that water penetration to the binding region is a common mechanism for all constructs. However, we find that the pathway enabling binding site hydration is not the same in all of them (see below), just as it was not the same in all the release paths identified by the Markov State Model analysis of the wild type protein (32) where several alternative pathways for hydration of the binding site were identified. In particular, in the wild type hDAT in PIP2 membrane the main (highest flux) pathway involved the opening of the intracellular gates formed by R60, D436, R445, and E428 residues following interaction of the proximal N-terminus with IL4, but some pathways did not require it. We monitored the hydration mechanisms in the different constructs and conditions by the changes in the interactions between R60–D436, E428–R445, and K66–D345 in trajectories in which Na^+ is released from Na2 site. Remarkably, we find that the relative importance of the hydration pathways can change with conditions that change the modes of N-terminus association.

For the S/D system all three salt bridge interactions are broken before the release of the Na^+ from the Na2 site (Figure S6). In the R51W construct, the R60–D436 interaction breaks prior to Na+/Na2 release in all three trajectories in which Na+/Na2 release was observed, but E428–R445 breaks in only one of the 3 trajectories, whereas the K66–D345 interaction breaks in 2 trajectories before the release of Na^+ from the Na2 site (Figure S7). In the no-PIP2 system, the key R60–D436 interaction is broken in 7 out of 9 trajectories, E428–R445 is broken in 4 out of 9 trajectories, and K66–D345 is broken in 8 out of 9 trajectories before the release of Na^+ from Na2 site (Figure S8). As a result, for the no-PIP2 system, there is increased preference for the water penetration path formed between TM1a and IL3 enabled by breaking of the K66–D345 interaction (see red colored pathway in Figure 4, below). We observe, therefore, that in R51W and no-PIP2 constructs, the E428–R445 interaction is least likely to break before the release of Na+/Na2 compared to the other intracellular gates. We also find, as shown on Figure 2, that in the R51W and no-PIP2 systems the N-terminus/IL4 interaction is substantially lower compared to the wild type system with PIP2. Taken together, our data suggest that the preference for a specific water penetration path changes in response to the different modes of N-terminus/IL4 association that result from mutations or PIP2 depletion. To obtain the mechanistic details of these differences

related to the N-terminus interactions that sustain the ability of Na+/Na2 release in the absence of PIP2 to an extent comparable (9/50 vs. 12/50) to the wild type simulated in PIP2-containing membranes (32), we used the MSM analysis to obtain a kinetic model for the Na+/Na2 release process under these conditions.

Kinetics of the inward release of Na^+ from the Na2 site in the PIP2-depleted membranes

To build the MSM for the no-PIP2 system, we followed the same protocol as described previously for the WT hDAT in PIP2-containing membranes (see Methods and ref. (32)) to enable direct comparison of the results. Thus, the reduced conformational space was generated with the tICA method (see Methods) utilizing the same set of parameters as before (32) (Table S3). The tICA energy landscape (Figure 3B) was obtained by projecting all the conformations from all the trajectories onto the first two tICA reaction coordinates. Visualization of conformations belonging to different regions of the tICA energy landscape revealed that this landscape, unlike the one for PIP2-containing membrane conditions (shown in Figure 3A), could be divided into only two (rather than three) regions in terms of the location of the Na+/Na2 ion: one in which the Na+/Na2 is still bound in the Na2 site, and the other in which the Na+/Na2 is already released (Figure 3B). Thus, this tICA space does not contain a region representing an intermediate state as seen in the wild type hDAT system in PIP2-enriched membranes (Figure 3C), when the Na+/Na2 that had left the binding site maintained an interaction with the E428 side chain freed from the E428–R445 interaction (32). Consequently, the results suggest that the change in N-terminus interactions due to PIP2 depletion directly affects this gate. This is consistent with our finding summarized in Fig. 2 showing a major reduction in the interactions of the N-terminus with IL4 in the absence of PIP2, and a more stable R445–E428 gate in the absence of PIP2 (Figure 3D, see also Figure S2).

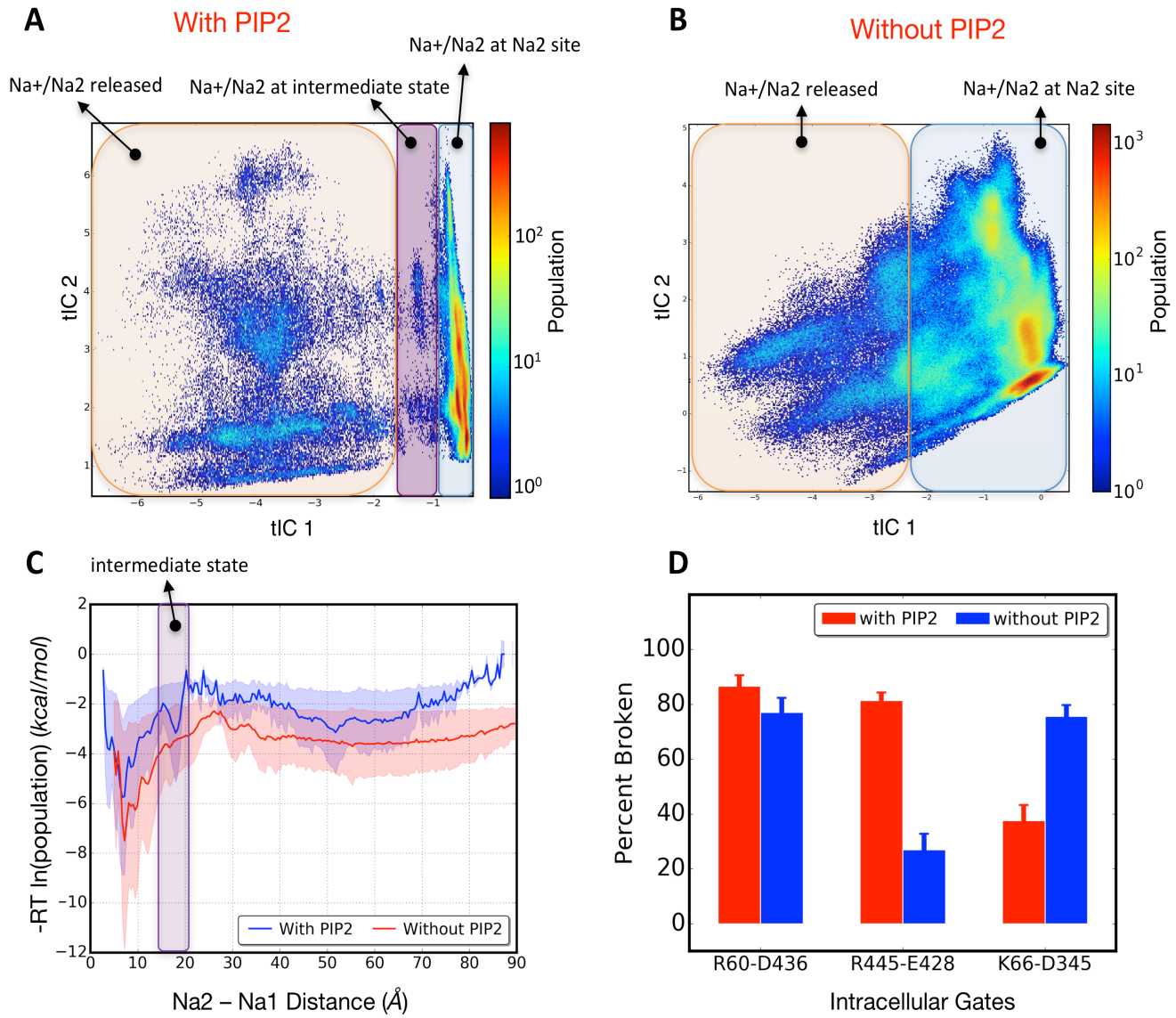

Figure 3. **hDAT tICA space in presence and absence of PIP2 lipids**. (**A** and **B**) Population-weighted tICA landscape for hDAT trajectories in PIP2-containing membranes (A) and for the no-PIP2 system (B). For each system, all of the conformations in all of the 50 trajectories are projected on the space of the tICA 1st and 2nd eigenvectors. Regions differing with respect to the location of Na+/Na2 are highlighted on the tICA landscape with transparent boxes of different colors. (**C**) All the conformations are projected on the reaction coordinate based on Na+/Na2 distance from sodium at site Na1, and the free energy (ΔG) is population-based and is calculated as [ΔG=-RT ln(population)]. The intermediate state is highlighted by the magenta box; note the absence of a distinct minimum in the absence of PIP2 (red line). Error bars (shown as transparent shades) are calculated using the bootstrap method on 100 blocks of frames with 160 ns time range that are randomly extracted from all 50 trajectories. (**D**) Comparing percent of broken interactions of intracellular gates in the control simulation (PIP2-containing membrane) (red bars) and in the no-PIP2 system (blue bars) averaged over all 50 trajectories of each construct. Error bars are calculated using the bootstrap method by randomly selecting 50 trajectories (with replacement method) and repeating the process for 1000 iterations.

To build the MSM from the 2D tICA landscape in Fig. 3B, we followed the same protocol as before (32) to obtain the *implied time scales* plot (see Methods). As shown in Figure S9 (*left panel*),

Markovian behavior of the system is observed after a lag time of ~80 ns, therefore the transition probability matrix (TPM) (see Methods) at 80 ns lag time was selected for all subsequent analyses of the no-PIP2 system. Mapping all microstates on the tICA landscape and coloring them based on the first MSM eigenvector (i.e., the first TPM eigenvector, shown in Figure S10) reveals that Na+/Na is still bound in microstates with positive sign (red circles in Figure S10), whereas the microstates with negative sign (blue circles in the Figure S10) have released the Na+/Na2 to the intracellular environment. Since the state population flows from the positive to negative states, the first MSM eigenvector is seen to capture the overall release kinetics of the Na+/Na2. The implied time-scale equation (see Methods) shows that this relaxation mode is characterized by time-scales of ~ 1.1μs, comparable to the previously reported kinetics for hDAT in the PIP2-containing membranes (~ 800 ns) (32) (Figure S9).

To compare the mechanisms of sodium release from the Na2 site of the WT hDAT in PIP2-containing vs PIP2-depleted membranes, we used the same transition path theory (TPT) analysis (see Methods) to obtain the most probable release pathways of Na+/Na2, and quantified the flux associated with each of these on a macrostate–based MSM using 15 macrostates as before (32). Similar to the WT in PIP2-containing membranes, in the no-PIP2 system the first 10 pathways identified by the TPT analysis contribute most (here ~80%) of the total flux between Na+/Na2 bound states and Na+/Na2 released states (highlighted in Figure 4; see Table S5 for quantification of fluxes).

The structural context of the pathways is shown in Figure 4. The first major pathway for the release of Na+/Na2 in the no-PIP2 system contributes ~40% of the total flux and is formed when both the R60–D436 and the E428–R445 gates are closed, but the K66–D345 is open (highlighted in the transparent red box in Figure 4). In sharp contrast to release in the PIP2-enriched system in which this is a minor pathway that contributes only ~13% of the total flux.

The second major pathway in the no-PIP2 system is enabled when both R60–D436 and E428–R445 gates are broken, but R60 is now able to form interactions with E428 (Figure 4, green box). This pathway contributes ~32% to the total flux. Notably, this was the major Na+/Na2 release pathway in the presence of PIP2, contributing about 48% percent of the total flux. But because R60 (or R445) is interacting with E428 here in the absence of PIP2, the intermediate state cannot form. The third major pathway in the no-PIP2 system is formed when the R60–D436 gate is broken and the N-terminus moves closer to IL2. The intracellular gate interaction E428–R445 is still maintained (Figure 4, blue box). In the presence of PIP2, this pathway contributes about ~39% to the total flux, but in the no-PIP2 system the contribution is reduced to 28%. Importantly, a major difference is that in the presence of PIP2, R60 is seen to be engaged in PIP2-mediated interactions with several positively charged residues from IL2 (K257, K260, K264), whereas in the no-PIP2 system the association between the N-terminus and the IL2 region still permits interactions between R60 and D68 and/or D385 (see macrostate 3 in Fig. 4 and Fig. S12).

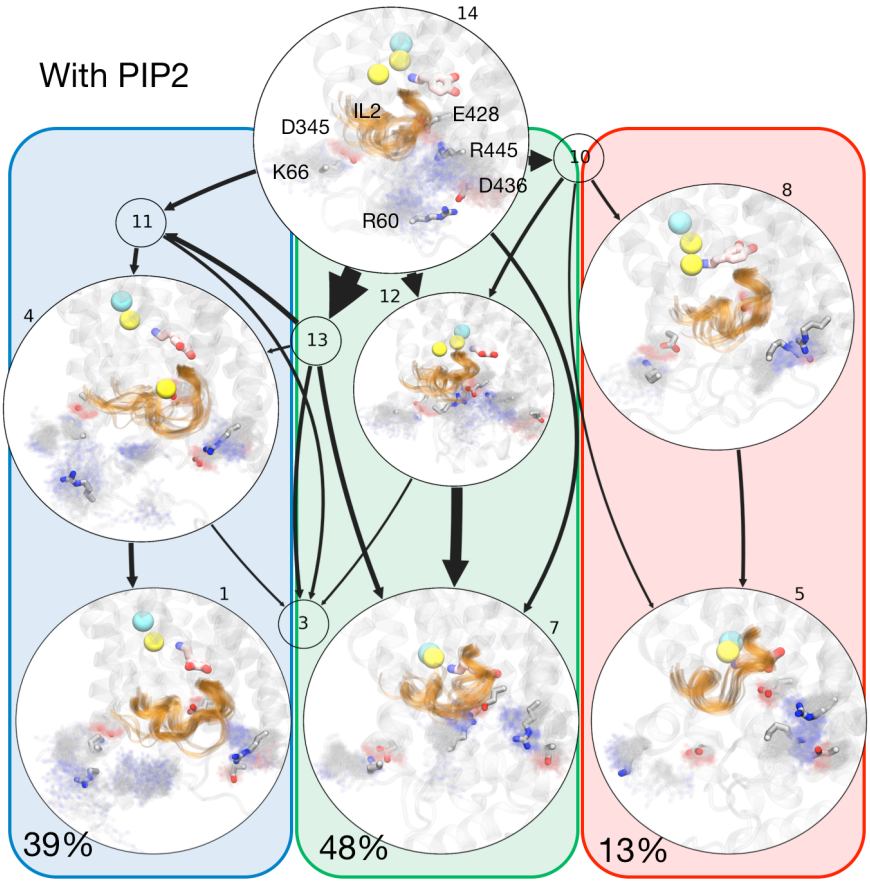
With PIP2
14
D345
IL2
E428
R445
K66
D436
R60
10
11
8
12
4
13
1
3
7
5
39%
48%
13%

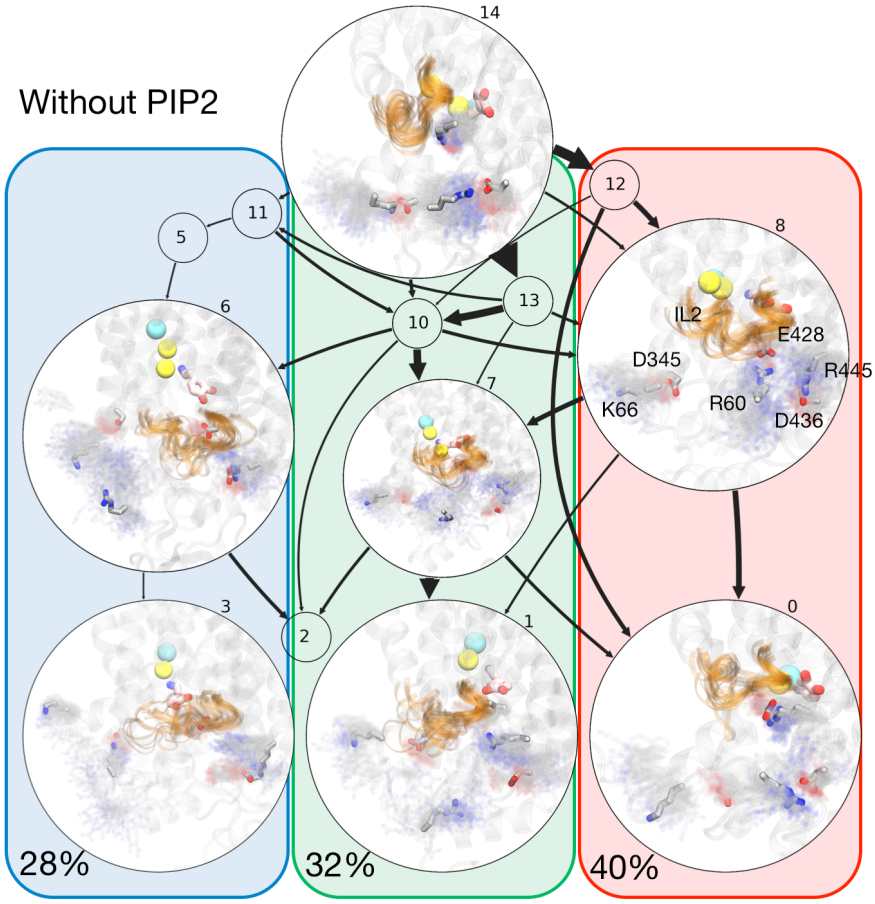
Without PIP2
14
12
11
5
8
13
6
10
IL2
E428
D345
R445
K66
R60
D436
7
3
2
1
0
28%
32%
40%

Figure 4. Comparison of Na+/Na2 release pathways calculated in PIP2-enriched and PIP2-depleted membranes. Results from the transition path theory (TPT) analysis for the release of Na+/Na2 to intracellular environment by the wild-type hDAT in PIP2-containing membranes (top) and in PIP2-depleted membranes (lower) systems. Arrow thickness represents relative flux for each transition. For some macrostates, a representative conformation is shown with IL2 highlighted in orange (cartoon representation) on the transparent structure of hDAT. Density representation of the residues forming intracellular gates are shown as fuzzy background gray colors and the most probable location of these residues are highlighted with licorice representation and labeled in some macrostates for reference. Dopamine is shown in pink licorice and sodium and chloride ions in yellow and cyan spheres, respectively. Red, green, and blue boxes highlight the three major release pathways of Na+/Na2; numbers indicate the fraction of flux carried by each major pathway.

Overall, the TPT analysis shows that the preference ranking of the various release pathways, which we quantified by calculating fluxes, is strongly affected by the PIP2 lipids. The increased stability of the E428–R445 gate in the no-PIP2 conditions leads to both the elimination of the intermediate state, and the reduction of Na+/Na2 release flux in what pathway in the presence of PIP2. Conversely, the destabilization of the K66–D345 gate resulting from the increased dynamics of the N-terminus (Figure S11) in the absence of PIP2, enhances Na+/Na2 release flux through a pathway that was only marginally active in the presence of PIP2 (the major pathway highlighted in red box). Taken together, these results suggest that release of the Na^+ from the Na2 site is maintained although N-terminus interaction patterns are modified in the absence of PIP2 lipids. This early mechanistic step in the uptake process is thus preserved in a time-scale that is comparable to that calculated in the same manner for hDAT in PIP2-containing membranes. Notably, this is achieved through release pathways that have a different probability ranking compared to the mechanism in PIP2-enriched membranes.

Discussion

The understanding gained from continuing investigations of the molecular mechanisms underlying the vital role of human DAT in signal transduction have profited much from the availability of structurally rather simpler prototypes of the NSS such as the bacterial analog LeuT (a leucine and alanine transporter), for which the crystallographic data provided the first structural basis for detailed molecular studies (see Refs. (16,39)). When the striking fold-similarity of LeuT to the eukaryotic and human neurotransmitter transporters such as DAT was established (40,41), it enabled major progress in understanding the functional mechanism as documented in a very large number of publications (for a review see (42)). It became clear, however, that various physiologically important mechanisms that eukaryotic transporters such as DAT and SERT have acquired through evolution involve allosteric coupling to their environment that differentiate them from the structurally simpler bacterial analogs. In a large number of studies (20,22,24-26,29,30,32,36,43-50) to which we have contributed findings from both computation and experiments, these new functions of the eukaryotic transporters – such as regulation by lipids, by phosphorylation, and the observed efflux phenotype –have been shown to be mechanistically modulated by defined structural elements, especially the relatively long N- and C-terminal segments that are found exclusively in this class, and not in bacterial counterparts (41). These intracellularly located N- and C-terminal segments are the most divergent structural units within the NSS family proteins ranging in size from just a few (~10) amino acids (in bacterial members, such as LeuT) to segments >60 residues (N-terminus of eukaryotic NSS such as DAT, SERT, see (27,41)).

The functional readout we used for the mechanistic impact of the various modes of gate opening and paths of water penetration on functional mechanism of DAT is the release of the Na+/Na2 ion, which is a key first step initiating the substrate translocation (33,34). The interaction of the hDAT N-

terminus with the intracellular regions of the transporter were quantified for the various constructs and conditions in terms of specific interaction modes of the distal and the proximal segments of the N-terminus. The results show that changes in the modes of interaction stemming from N-terminus mutations and PIP2 depletion, are directly associated with stabilization/destabilization of intracellular gates. This is evidenced in the stabilization of the E428–R445 interaction in the absence of PIP2, compared to its destabilization in the presence of PIP2 due to a strong interaction of the N-terminus with IL4 (30). The opening probabilities of the corresponding water penetration paths echoes these differences, enhancing that of the TM1a/IL3 pathway over the N-term/IL4 pathway in one case, and switching them in the other (see Figure 5A).

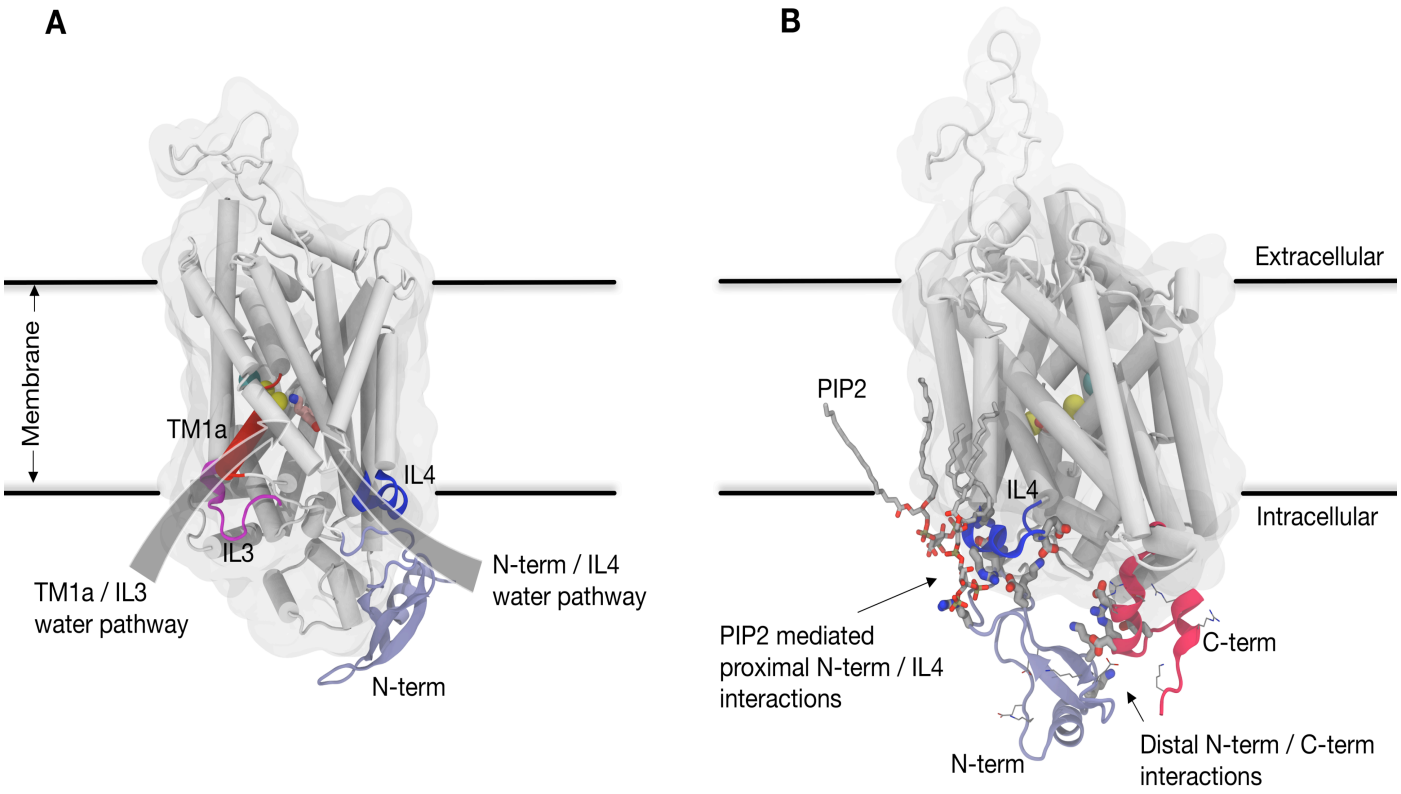

Figure 5. Illustration of effects of different modes of N-terminus interactions on functional phenotypes. (**A**) Representation of two water penetration pathways from the intracellular side of the hDAT. The N-terminus/IL4 water pathway is the main water penetration path in the wild-type in the presence of PIP2 lipids. In the absence of PIP2, the N-terminus/IL4 water (blue) penetration pathway is impaired, and hydration of the binding site is achieved primarily through another water pathway formed between TM1a and IL3 (red). (**B**) Representation of conditions linked to the efflux function of hDAT. The interaction of the proximal N-terminus with IL4 (blue) is mediated by PIP2 lipids, and the distal part of the N-terminus engages with the C-terminus (red). All charged residues are shown for both N-terminus and C-terminus with thin licorice; charged residues engaged in interactions between N-terminus and either IL4 or the C-terminus, are highlighted with thick licorice. Dopamine is shown in the S1 binding site (in pink), sodium ions are shown as yellow spheres, and the chloride ion is in cyan.

This reordering of water pathway probabilities provides a clear mechanistic explanation for an apparent conundrum regarding the relative importance of the N-terminus/IL4 interaction. Because the disruption of the E428–R445 gate was found to be one of the major mechanistic triggers for the Na^+

release from the Na2 site in PIP2-containing membranes (30), and under no-PIP2 conditions this interaction is reduced, it might have appeared that the reduced N-terminus/IL4 interactions would interfere with the release of Na^+ from the Na2 site and impair uptake function. This is not what is observed experimentally, as the uptake function of hDAT is not impaired by PIP2 depletion from membrane (Table 1). This is fully consistent with our findings that several release pathways are triggered by the rich spectrum of interaction of the N-terminus, albeit with different probabilities (i.e., contributions to the flux of Na^+ release) (32). Our results (Fig. 2) show how these modes of interaction change under the different conditions for the various mutant constructs, and the MSM analysis for the no-PIP2 condition shows how the probabilities of the different pathways associated with the different modes of interaction do change to produce the experimentally observed phenotypes, so that water penetrates through alternative channels, e.g., the TM1a/IL3 channel (Figure 5A), to activate alternative Na+/Na2 release pathways.

The different modes of N-terminus interaction with the membrane recorded for the various constructs lead to both repositioning, and to changes in the strengths of associations with the other regions of the transporter. In turn, these interactions reorganize the dynamics of the transporter, supporting different structure-based functional phenotypes. An interesting difference in phenotype regulation by the N-terminus is evident in the independent regulation by the PIP2 content of the membrane, of the inward (uptake) and reverse (efflux) dopamine transport by DAT. The biological relevance of a change in AMPH-induced dopamine efflux (a phenotype not shared by the bacterial analogs such as LeuT, which lack the long N-terminus) separately from a change in the uptake of dopamine became clear with the discovery of several *de novo* mutations in the human DAT (hDAT) (9-11,15,37) . These mutations are linked to neurological disorders and affect the efflux phenotype. Indeed, mutations such as R51W (37), and removal of PIP2 lipids from membrane have been shown to reduce AMPH-induced efflux (29). Importantly, our results (Figure 2) show that both of these conditions lead to major changes in the pattern of N-terminus interactions with the rest of transporter molecule, and especially the reduction of N-terminus/IL4 interactions. Thus, N-terminus/IL4 interactions are mostly enabled by PIP2 mediated interactions between R51 (in the N-terminus) and R443 (in IL4), and we found that the R51W mutant also has a high interaction score with IL4 (Figure 2), but this is helped by the distal N-terminus (rather than the proximal, see Figure S1). This change in mode of interaction for R51W contrasts with the effect we observed for the introduction of the phosphomimic S-to-D mutations (S/D hDAT construct), which had been shown experimentally to possess basal efflux activity even in the absence of amphetamine (22). We found its N-terminus/IL4 interactions to be the least perturbed compared to the wild type, but also a remarkably large association with the C-terminus. When the N-terminus/IL4 interactions are eliminated or reduced by specific mutations (such as the R51W construct), or by removal of PIP2 from the membrane, they produce major reductions in efflux (Table 1). Indeed, the requirement for PIP2 lipids for the efflux process has been demonstrated as well for SERT (e.g., see (51)), consistent with the role of the charged residues in the N-terminus of the eukaryotic NSS proteins in the observed functional phenotypes. Thus, K3/5A with its drastically reduced charge also has reduced efflux. Further observations about the role of the charges in the N-terminus point to the interactions with the C-terminus that are very high for the S/D construct (which exhibits robust, AMPH-independent efflux), but are the lowest for the K3/5A construct in which efflux is impaired. Notably, the increase in the N-terminus/C-terminus association in the S/D construct is due primarily to ionic interactions formed by the Asp residues in the distal part of the N-terminus (residues 1-22) with basic residues in the C-term (e.g., D7, D12, and D13 with R615 in the C-terminus), and these interactions would be eliminated in the truncated N-terminus construct (ΔN22) that was shown to maintain its uptake activity (22), but to have drastically impaired efflux activity, further supporting the separation of modes of interactions affecting efflux from those affecting mainly transport.

It is tempting to speculate that the reduction of proximal N-terminus/IL4 interactions in constructs with low efflux activity and in PIP2-depleted membranes, combined with the reduction in

distal N-terminus/C-terminus interactions in efflux-inhibiting K3/5A and increase in distal N-terminus/C-terminus interactions in efflux-promoting S/D construct, might suggest that specific combinations of interaction modes, and a robust ability to interact with the C-terminus, are required for efflux (Figure 5B). This is also consistent with the observation that palmitoylation of the C-terminus reduces efflux, presumably by reducing N-terminus phosphorylation (52,53) and thus interaction with the C-terminus, whereas Ca2+/calmodulin-dependent protein kinase II was suggested to induce efflux by binding to the distal C-terminus of hDAT and phosphorylating the serine residues in the distal N-terminus (26).

Conclusions

We have identified elements of the complex roles of the N-terminus and C-terminus of the eukaryotic NSS transporters in mechanisms that are not available in the homologous bacterial transporters. By showing that mechanistic elements in a required initial step (Na+/Na2 release) of substrate translocation result in different, alternative pathways, with different probabilities, we identified a mechanistic basis for the separation of phenotypes observed for different constructs and conditions of the dopamine transporter. Thus, the MSM model we have developed for the kinetics of Na+/Na2 release explains uptake insensitivity to PIP2 while suggesting possible requirements for the PIP2-sensitive efflux. The importance of such models in understanding mechanism of function for the SLC6 neurotransmitter transporters is underscored by the correspondence between the observed changes in mechanistic steps quantified by this model, to specific experimentally observed phenotypes and the mechanistic resolution of a conundrum posed by experimental findings that have been debated but had remained open. Specifically, this was achieved here by (1)-our demonstration that the distal and proximal segments of the N-terminus utilize differently the important contribution of PIP2 lipids to the uptake and efflux mechanisms of hDAT, (2)-identifying alternative pathways of water penetration that can lead to Na+/Na2 release showing how hDAT overcomes the effects of absence of PIP2 to maintain uptake although efflux is impaired, and (3)-showing how truncation of residues 1-22 of the hDAT terminus are expected to affect differentially the uptake and efflux functions of the transporter, a characteristic shared with the serotonin transporter SERT.

Methods

System preparation. The molecular model of full-length wild type hDAT used in this study is the same as described and investigated earlier (32). The R51W and K3A+K5A constructs were prepared by introducing the mutations in the wild type hDAT model using VMD mutator plugin (54). To build the S/D mutant (simultaneous mutations of S2, S4, S7, S12, and S13 residues to Asp), we combined, using Modeller version 9v1 (55), the 57-620 residue stretch from the wild type hDAT structure with the structural model of the 1-57 S/D segment elaborated and described previously (20).

The full length models of the hDAT constructs R51W, K3A+K5A (heretofore referred to as "K3/5A"), and S/D were inserted into the same pre-equilibrated compositionally asymmetric bilayer membrane used for MD simulations of the wild type hDAT (32). This lipid bilayer was designed to mimic a neuronal cell plasma membrane and contains 5% PI(4,5)P_2 lipid on the intracellular leaflet of the bilayer (see Table S1 for membrane lipid composition). For the simulations of the wild type hDAT in PI(4,5)P_2-depleted membrane environment, all the PI(4,5)P_2 lipids in the bilayer were changed to POPE lipids, as done previously (30). All the hDAT-membrane systems were solvated in a 150 mM K^+Cl^- TIP3P water solution with ions added for neutrality, resulting in a final atom count of ~150,000.

Molecular dynamics simulations. All-atom molecular dynamics (MD) simulations were carried out using the same scheme as described earlier for the wild type hDAT in PI(4,5)P_2-enriched membranes

(32). Briefly, using NAMD software version 2.10 (56), the systems first were equilibrated following the same multi-step equilibration protocol used previously (32) during which the backbone of the protein was first fixed, then harmonically restrained, and finally released. After this equilibration phase, the velocities of all the atoms in the system were reset (at T=310K using random number seed) and 50 independent ~1μs long unbiased MD simulations were carried out using the ACEMD software (57) resulting in a cumulative MD simulation time of ~50 μs per system. Complete details of the simulation protocol employed are documented in reference (32).

Calculation of the interaction strengths. To obtain a measure of interaction between N-terminus and other intracellular regions of hDAT we counted the number of interactions between charged residues from the N-terminus and the intracellular loop regions. The number of interactions was quantified for a cutoff distance of 7 Å between interacting residue pairs from head group atoms of the N-terminus and of intracellular domain residues (using N_ξ for Lys, C_ξ for Arg, C_δ for Glu, and C_γ for Asp). Total number of interactions is then divided by total number of frames to obtain the "interaction strength" represented in Figure 2. The residues included are specified in Table S2. All 50 trajectories for each construct were used for these calculations, with the first 500 ns of each trajectory considered an equilibration phase so that only the 500-940 ns time interval from each trajectory was used to ensure that the total number of frames used for the analysis was the same for the interaction strength calculations in each trajectory.

Markov State based quantitative kinetic model construction. We used the Markov State Model (MSM) approach to analyze the trajectories in the absence of PIP2 lipids and build quantitative kinetic models of sodium release from the Na2 site for comparison with the kinetics and pathways calculated in the presence of PIP2 in Ref. (32). Therefore, we have followed here the same protocol as described in detail in Ref. (32). Such quantitative kinetic models provided by Markov State Models (MSMs) (58,59)·(60) have been widely applied in protein folding studies (61,62) and MSM based kinetic models predictions have been validated experimentally (63,64). We and others have used MSMs combined with reactive flux analysis, such as transition path theory (TPT) analysis to obtain key mechanistic insights into functions of membrane proteins (32,65,66). The three main components for achieving quantitative MSM-based kinetic models are briefly reviewed below.

1. Dimensionality reduction using tICA. Reducing the dimensionality of a system as large and complex as the membrane-immersed hDAT is necessary in order to construct an interpretable kinetic model. A natural choice of suitable reaction coordinates is for those that can project the conformational space of the system along its *slowest* reaction coordinate, as this reaction coordinate will capture most of the conformational heterogeneity during the time-course of the simulation (67). The *time-structure based Independent Component Analysis* (tICA) method was developed recently for this purpose of capturing the slowest reaction coordinate of a system (68-70). Briefly, the tICA method involves a transformation that utilizes two matrices constructed from the trajectory data: the covariance matrix **C**, and a time-lagged covariance matrix $\boldsymbol{C_{TL}}$. The slowest reaction coordinates of a system are then defined by eigenvectors of the generalized eigenvalue problem: $\boldsymbol{C_{TL}}\mathbf{V} = \mathbf{CV\Lambda}$, where $\mathbf{\Lambda}$ and **V** are the eigenvalue and eigenvector matrices, respectively. The eigenvectors corresponding to the largest eigenvalues identify the slowest reaction coordinates. Here we used a lag time of 16 ns to construct the time-lagged covariance matrix $\boldsymbol{C_{TL}}$, and the tICA parameters were chosen as before for the hDAT molecular system (32), to measure a) the dynamics of the Na^+ ion from the Na2 site, termed Na+/Na2, and b) the dynamics of intracellular gates formed between residues R60, D436, R445, E428 (Table S3).

2. Markov Model construction. The conformational transitions of biomolecular systems where the time between transitions is long enough can be modeled as Markov chains (58) in which transitions among states depend only on the current state of the system (i.e., Markovian behavior). Such Markov models provide powerful tools for outcome prediction by enabling the extraction of long time-scale information from multiples of short time-scale events.

Two components needed for the construction of such a Markov model are: an ensemble of *microstates* of the system, and of the transitions among these microstates (71). Microstates are defined by clustering the conformational space of the system into several basins using automated clustering algorithms like *K*-means or *K*-centers, and is most practical if performed in a dimensionality-reduced space such as the one obtained from the tICA transformation. The transitions among the microstates are calculated for a particular time interval between each of the transitions (so called lag-time) and stored in the *transition count matrix*. By row-normalizing the transition count matrix one obtains the *transition probability matrix* (TPM). To validate Markovian behavior, the TPMs are constructed for multiple lag times and the relaxation timescales of the system are extracted by using the relation:

$$\tau_i = \frac{\tau'}{\ln \lambda_i}$$

where τ' is the lag-time used for building the TPM, λ_i is the ith eigenvalue of the transition probability matrix, and the resulting τ_i is the so-called *implied timescale* corresponding to the ith relaxation mode of the system. The system is considered to be Markovian if the behavior is such that τ_i is independent of τ'; the corresponding TPM is a *Markovian* TPM that contains all the information about the thermodynamics and kinetics of the system. Thermodynamic information is stored in the first eigenvector (which has an eigenvalue of 1). Information about kinetics is stored in the subsequent (second, third, etc.) eigenvectors, with the second eigenvector (corresponding to the second largest eigenvalue) capturing the slowest dynamics of the system, the third eigenvector capturing the second slowest dynamics, and so on.

Following the same protocols as described in detail in Ref. (32) for the construction of the Markov Models we discretized the reduced conformational space generated by the first two tICA reactions coordinates into 100 microstates (Figure S10) using the *K-means* clustering algorithm implemented in the MSMBuilder3 software (72). Transition probability matrices (TPMs) were constructed at several different lag times to obtain the implied time-scale plots shown in Figures S9, so that the one in which Markovian behavior is exhibited can be identified and chosen for further analysis.

3. Transition path theory analysis. In addition to the thermodynamics and kinetics information it contains, the Markovian TPM also contains mechanistic information for a dynamic system. An established means of revealing such mechanistic information inherent in the TPM is the Transition Path Theory (TPT) analysis that identifies the most probable flux pathways of the system (73). TPT provides such pathways by constructing a *flux matrix* from the Markovian TPM. This matrix conversion has been documented in detail (73,74) and its implementation is discussed in our previous publication (32). Although directly applicable to MSM in the microstate space (on the order of hundreds to thousands of states), TPT analysis is usually done on a *macrostate* MSM (on the order of tens of states) for a better visualization of flux pathways. Here we transitioned from the microstate–MSM to macrostate–MSM by using the Robust Perron Cluster Analysis ($PCCA^+$) algorithm (75) that lumps microstates into macrostates using the sign structure of the MSM eigenvectors (this assumes that microstates with the same signs, positive or negative, in the MSM eigenvectors, will have similar kinetics (76)). Using the $PCCA^+$ algorithm we obtained 15 macrostates and by applying the TPT analysis to these macrostates we obtained the most probable flux pathways for the system.

List of abbreviations: SLC6: solute carrier 6, NSS: neurotransmitter:sodium symporter, DAT: dopamine transporter, hDAT: human dopamine transporter, SERT: serotonin transporter, TM: transmembrane, MSM: Markov State Model, tICA: time-structure based independent component analysis, TPM: transition probability matrix, TPT: transition path theory

Declarations

Competing interests: The authors declare that they have no competing interests.

Funding: The work was supported by NIH Grants P01 DA012408, R01 DA041510 and in part U54 GM087519.

Authors' contributions: All authors contributed to conceiving the project and experimental design, A.M.R. did the analysis and carried out the MSM construction, G.K. carried out the MD simulations, all authors participated in the interpretation of results and in writing the manuscript.

Acknowledgments: The following computational resources are gratefully acknowledged: resources of the Oak Ridge Leadership Computing Facility (ALCC allocation BIP109) at the Oak Ridge National Laboratory, which is supported by the Office of Science of the U.S. Department of Energy under Contract No. DE-AC05-00OR22725; an allocation at the National Energy Research Scientific Computing Center (NERSC, repository m1710) supported by the Office of Science of the U.S. Department of Energy under Contract No. DE-AC02- 05CH11231; and the computational resources of the David A. Cofrin Center for Biomedical Information in the HRH Prince Alwaleed Bin Talal Bin Abdulaziz Alsaud Institute for Computational Biomedicine at Weill Cornell Medical College.

References

1. Broer, S., and Gether, U. (2012) The solute carrier 6 family of transporters. *Br J Pharmacol* 167, 256-278
2. Sulzer, D., Sonders, M. S., Poulsen, N. W., and Galli, A. (2005) Mechanisms of neurotransmitter release by amphetamines: a review. *Prog Neurobiol* 75, 406-433
3. Ng, J., Papandreou, A., Heales, S. J., and Kurian, M. A. (2015) Monoamine neurotransmitter disorders--clinical advances and future perspectives. *Nat Rev Neurol* 11, 567-584
4. Vaughan, R. A., and Foster, J. D. (2013) Mechanisms of dopamine transporter regulation in normal and disease states. *Trends Pharmacol Sci* 34, 489-496
5. Ritz, M. C., Lamb, R., and Kuhar, M. (1987) Cocaine receptors on dopamine transporters are related to self-administration of cocaine. *Science* 237, 1219-1223
6. Sulzer, D. (2011) How addictive drugs disrupt presynaptic dopamine neurotransmission. *Neuron* 69, 628-649
7. Shekar, A., Aguilar, J. I., Galli, G., Cozzi, N. V., Brandt, S. D., Ruoho, A. E., Baumann, M. H., Matthies, H. J., and Galli, A. (2017) Atypical dopamine efflux caused by 3, 4-methylenedioxypyrovalerone (MDPV) via the human dopamine transporter. *Journal of chemical neuroanatomy* 83, 69-74
8. Bowton, E., Saunders, C., Erreger, K., Sakrikar, D., Matthies, H. J., Sen, N., Jessen, T., Colbran, R. J., Caron, M. G., and Javitch, J. A. (2010) Dysregulation of dopamine transporters via dopamine D2 autoreceptors triggers anomalous dopamine efflux associated with attention-deficit hyperactivity disorder. *Journal of Neuroscience* 30, 6048-6057

9. Bowton, E., Saunders, C., Reddy, I. A., Campbell, N. G., Hamilton, P. J., Henry, L. K., Coon, H., Sakrikar, D., Veenstra-VanderWeele, J. M., Blakely, R. D., Sutcliffe, J., Matthies, H. J., Erreger, K., and Galli, A. (2014) SLC6A3 coding variant Ala559Val found in two autism probands alters dopamine transporter function and trafficking. *Transl Psychiatry* 4, e464
10. Hamilton, P. J., Campbell, N. G., Sharma, S., Erreger, K., Herborg Hansen, F., Saunders, C., Belovich, A. N., Sahai, M. A., Cook, E. H., Gether, U., McHaourab, H. S., Matthies, H. J., Sutcliffe, J. S., and Galli, A. (2013) De novo mutation in the dopamine transporter gene associates dopamine dysfunction with autism spectrum disorder. *Mol Psychiatry* 18, 1315-1323
11. Hansen, F. H., Skjorringe, T., Yasmeen, S., Arends, N. V., Sahai, M. A., Erreger, K., Andreassen, T. F., Holy, M., Hamilton, P. J., Neergheen, V., Karlsborg, M., Newman, A. H., Pope, S., Heales, S. J., Friberg, L., Law, I., Pinborg, L. H., Sitte, H. H., Loland, C., Shi, L., Weinstein, H., Galli, A., Hjermind, L. E., Moller, L. B., and Gether, U. (2014) Missense dopamine transporter mutations associate with adult parkinsonism and ADHD. *J Clin Invest* 124, 3107-3120
12. Mazei-Robison, M. S., Bowton, E., Holy, M., Schmudermaier, M., Freissmuth, M., Sitte, H. H., Galli, A., and Blakely, R. D. (2008) Anomalous dopamine release associated with a human dopamine transporter coding variant. *Journal of Neuroscience* 28, 7040-7046
13. Mergy, M. A., Gowrishankar, R., Gresch, P. J., Gantz, S. C., Williams, J., Davis, G. L., Wheeler, C. A., Stanwood, G. D., Hahn, M. K., and Blakely, R. D. (2014) The rare DAT coding variant Val559 perturbs DA neuron function, changes behavior, and alters in vivo responses to psychostimulants. *Proceedings of the National Academy of Sciences* 111, E4779-E4788
14. Ng, J., Zhen, J., Meyer, E., Erreger, K., Li, Y., Kakar, N., Ahmad, J., Thiele, H., Kubisch, C., and Rider, N. L. (2014) Dopamine transporter deficiency syndrome: phenotypic spectrum from infancy to adulthood. *Brain* 137, 1107-1119
15. Sakrikar, D., Mazei-Robison, M. S., Mergy, M. A., Richtand, N. W., Han, Q., Hamilton, P. J., Bowton, E., Galli, A., Veenstra-Vanderweele, J., Gill, M., and Blakely, R. D. (2012) Attention deficit/hyperactivity disorder-derived coding variation in the dopamine transporter disrupts microdomain targeting and trafficking regulation. *J Neurosci* 32, 5385-5397
16. Yamashita, A., Singh, S. K., Kawate, T., Jin, Y., and Gouaux, E. (2005) Crystal structure of a bacterial homologue of Na+/Cl--dependent neurotransmitter transporters. *Nature* 437, 215-223
17. Penmatsa, A., Wang, K. H., and Gouaux, E. (2013) X-ray structure of dopamine transporter elucidates antidepressant mechanism. *Nature* 503, 85-90
18. Malinauskaite, L., Quick, M., Reinhard, L., Lyons, J. A., Yano, H., Javitch, J. A., and Nissen, P. (2014) A mechanism for intracellular release of Na+ by neurotransmitter/sodium symporters. *Nat Struct Mol Biol* 21, 1006-1012
19. Kantcheva, A. K., Quick, M., Shi, L., Winther, A.-M. L., Stolzenberg, S., Weinstein, H., Javitch, J. A., and Nissen, P. (2013) Chloride binding site of neurotransmitter sodium symporters. *Proceedings of the National Academy of Sciences* 110, 8489-8494
20. Khelashvili, G., Doktorova, M., Sahai, M. A., Johner, N., Shi, L., and Weinstein, H. (2015) Computational modeling of the N-terminus of the human dopamine transporter and its interaction with PIP2-containing membranes. *Proteins: Structure, Function, and Bioinformatics* 83, 952-969
21. Fenollar-Ferrer, C., Stockner, T., Schwarz, T. C., Pal, A., Gotovina, J., Hofmaier, T., Jayaraman, K., Adhikary, S., Kudlacek, O., and Mehdipour, A. R. (2014) Structure and regulatory interactions of the cytoplasmic terminal domains of serotonin transporter. *Biochemistry* 53, 5444-5460
22. Khoshbouei, H., Sen, N., Guptaroy, B., Johnson, L., Lund, D., Gnegy, M. E., Galli, A., and Javitch, J. A. (2004) N-terminal phosphorylation of the dopamine transporter is required for amphetamine-induced efflux. *PLoS Biol* 2, E78

23. Moritz, A. E., Rastedt, D. E., Stanislowski, D. J., Shetty, M., Smith, M. A., Vaughan, R. A., and Foster, J. D. (2015) Reciprocal Phosphorylation and Palmitoylation Control Dopamine Transporter Kinetics. *J Biol Chem* 290, 29095-29105
24. Binda, F., Dipace, C., Bowton, E., Robertson, S. D., Lute, B. J., Fog, J. U., Zhang, M., Sen, N., Colbran, R. J., and Gnegy, M. E. (2008) Syntaxin 1A interaction with the dopamine transporter promotes amphetamine-induced dopamine efflux. *Molecular pharmacology* 74, 1101-1108
25. Cremona, M. L., Matthies, H. J., Pau, K., Bowton, E., Speed, N., Lute, B. J., Anderson, M., Sen, N., Robertson, S. D., and Vaughan, R. A. (2011) Flotillin-1 is essential for PKC-triggered endocytosis and membrane microdomain localization of DAT. *Nature neuroscience* 14, 469-477
26. Fog, J. U., Khoshbouei, H., Holy, M., Owens, W. A., Vaegter, C. B., Sen, N., Nikandrova, Y., Bowton, E., McMahon, D. G., and Colbran, R. J. (2006) Calmodulin kinase II interacts with the dopamine transporter C terminus to regulate amphetamine-induced reverse transport. *Neuron* 51, 417-429
27. Khelashvili, G., and Weinstein, H. (2015) Functional mechanisms of neurotransmitter transporters regulated by lipid–protein interactions of their terminal loops. *Biochimica et Biophysica Acta (BBA)-Biomembranes* 1848, 1765-1774
28. Pizzo, A. B., Karam, C. S., Zhang, Y., Yano, H., Freyberg, R. J., Karam, D. S., Freyberg, Z., Yamamoto, A., McCabe, B. D., and Javitch, J. A. (2013) The membrane-raft protein Flotillin-1 is essential in dopamine neurons for amphetamine-induced behavior in Drosophila. *Molecular psychiatry* 18, 824
29. Hamilton, P. J., Belovich, A. N., Khelashvili, G., Saunders, C., Erreger, K., Javitch, J. A., Sitte, H. H., Weinstein, H., Matthies, H. J., and Galli, A. (2014) PIP2 regulates psychostimulant behaviors through its interaction with a membrane protein. *Nat Chem Biol* 10, 582-589
30. Khelashvili, G., Stanley, N., Sahai, M. A., Medina, J., LeVine, M. V., Shi, L., De Fabritiis, G., and Weinstein, H. (2015) Spontaneous inward opening of the dopamine transporter is triggered by PIP2-regulated dynamics of the N-terminus. *ACS Chem Neurosci* 6, 1825-1837
31. Cheng, M. H., and Bahar, I. (2015) Molecular mechanism of dopamine transport by human dopamine transporter. *Structure* 23, 2171-2181
32. Razavi, A. M., Khelashvili, G., and Weinstein, H. (2017) A Markov state-based quantitative kinetic model of sodium release from the dopamine transporter. *Scientific reports* 7, 40076
33. Shi, L., Quick, M., Zhao, Y., Weinstein, H., and Javitch, J. A. (2008) The mechanism of a neurotransmitter:sodium symporter--inward release of Na+ and substrate is triggered by substrate in a second binding site. *Mol Cell* 30, 667-677
34. Tavoulari, S., Margheritis, E., Nagarajan, A., DeWitt, D. C., Zhang, Y.-W., Rosado, E., Ravera, S., Rhoades, E., Forrest, L. R., and Rudnick, G. (2016) Two Na+ sites control conformational change in a neurotransmitter transporter homolog. *Journal of Biological Chemistry* 291, 1456-1471
35. Kern, C., Erdem, F. A., El-Kasaby, A., Sandtner, W., Freissmuth, M., and Sucic, S. (2017) The N Terminus Specifies the Switch between Transport Modes of the Human Serotonin Transporter. *Journal of Biological Chemistry* 292, 3603-3613
36. Buchmayer, F., Schicker, K., Steinkellner, T., Geier, P., Stübiger, G., Hamilton, P. J., Jurik, A., Stockner, T., Yang, J.-W., and Montgomery, T. (2013) Amphetamine actions at the serotonin transporter rely on the availability of phosphatidylinositol-4, 5-bisphosphate. *Proceedings of the National Academy of Sciences* 110, 11642-11647
37. Cartier, E., Hamilton, P., Belovich, A. N., Shekar, A., Campbell, N. G., Saunders, C., Andreassen, T. F., Gether, U., Veenstra-Vanderweele, J., Sutcliffe, J. S., Ulery-Reynolds, P. G., Erreger, K., Matthies, H. J., and Galli, A. (2015) Rare Autism-Associated Variants Implicate Syntaxin 1 (STX1 R26Q) Phosphorylation and the Dopamine Transporter (hDAT R51W) in Dopamine Neurotransmission and Behaviors. *EBioMedicine* 2, 135-146

38. McGibbon, R. T., Beauchamp, K. A., Harrigan, M. P., Klein, C., Swails, J. M., Hernández, C. X., Schwantes, C. R., Wang, L.-P., Lane, T. J., and Pande, V. S. (2015) MDTraj: A modern open library for the analysis of molecular dynamics trajectories. *Biophysical journal* 109, 1528-1532
39. Penmatsa, A., and Gouaux, E. (2013) How LeuT shapes our understanding of the mechanisms of sodium-coupled neurotransmitter transporters. *J Physiol* 592, 863-869
40. Gether, U., Andersen, P. H., Larsson, O. M., and Schousboe, A. (2006) Neurotransmitter transporters: molecular function of important drug targets. *Trends Pharmacol Sci* 27, 375-383
41. Beuming, T., Shi, L., Javitch, J. A., and Weinstein, H. (2006) A comprehensive structure-based alignment of prokaryotic and eukaryotic neurotransmitter/Na+ symporters (NSS) aids in the use of the LeuT structure to probe NSS structure and function. *Molecular pharmacology* 70, 1630-1642
42. Li, J., Wen, P.-C., Moradi, M., and Tajkhorshid, E. (2015) Computational characterization of structural dynamics underlying function in active membrane transporters. *Current opinion in structural biology* 31, 96-105
43. Sweeney, C. G., Tremblay, B. P., Stockner, T., Sitte, H. H., and Melikian, H. E. (2017) Dopamine Transporter Amino and Carboxyl Termini Synergistically Contribute to Substrate and Inhibitor Affinities. *Journal of Biological Chemistry* 292, 1302-1309
44. Moritz, A. E., Foster, J. D., Gorentla, B. K., Mazei-Robison, M. S., Yang, J.-W., Sitte, H. H., Blakely, R. D., and Vaughan, R. A. (2013) Phosphorylation of dopamine transporter serine 7 modulates cocaine analog binding. *Journal of Biological Chemistry* 288, 20-32
45. Foster, J. D., Yang, J.-W., Moritz, A. E., ChallaSivaKanaka, S., Smith, M. A., Holy, M., Wilebski, K., Sitte, H. H., and Vaughan, R. A. (2012) Dopamine transporter phosphorylation site threonine 53 regulates substrate reuptake and amphetamine-stimulated efflux. *Journal of Biological Chemistry* 287, 29702-29712
46. Sucic, S., Dallinger, S., Zdrazil, B., Weissensteiner, R., Jørgensen, T. N., Holy, M., Kudlacek, O., Seidel, S., Cha, J. H., and Gether, U. (2010) The N terminus of monoamine transporters is a lever required for the action of amphetamines. *Journal of Biological Chemistry* 285, 10924-10938
47. Li, J., Shaikh, S. A., Enkavi, G., Wen, P.-C., Huang, Z., and Tajkhorshid, E. (2013) Transient formation of water-conducting states in membrane transporters. *Proceedings of the National Academy of Sciences* 110, 7696-7701
48. Shaikh, S. A., and Tajkhorshid, E. (2010) Modeling and dynamics of the inward-facing state of a Na+/Cl− dependent neurotransmitter transporter homologue. *PLoS computational biology* 6, e1000905
49. Zomot, E., Gur, M., and Bahar, I. (2015) Microseconds simulations reveal a new sodium-binding site and the mechanism of sodium-coupled substrate uptake by LeuT. *Journal of Biological Chemistry* 290, 544-555
50. Cheng, M. H., and Bahar, I. (2014) Complete mapping of substrate translocation highlights the role of LeuT N-terminal segment in regulating transport cycle. *PLoS computational biology* 10, e1003879
51. Buchmayer, F., Schicker, K., Steinkellner, T., Geier, P., Stubiger, G., Hamilton, P. J., Jurik, A., Stockner, T., Yang, J. W., Montgomery, T., Holy, M., Hofmaier, T., Kudlacek, O., Matthies, H. J., Ecker, G. F., Bochkov, V., Galli, A., Boehm, S., and Sitte, H. H. (2013) Amphetamine actions at the serotonin transporter rely on the availability of phosphatidylinositol-4,5-bisphosphate. *Proc Natl Acad Sci U S A* 110, 11642-11647
52. Foster, J. D., and Vaughan, R. A. (2016) Phosphorylation mechanisms in dopamine transporter regulation. *Journal of chemical neuroanatomy* 83, 10-18
53. Rastedt, D., Foster, J., and Vaughan, R. (2015) Dopamine transporter expression and transport capacity is regulated by palmitoylation. *The FASEB Journal* 29, 768.764

54. Humphrey, W., Dalke, A., and Schulten, K. (1996) VMD: visual molecular dynamics. *Journal of molecular graphics* 14, 33-38
55. Webb, B., and Sali, A. (2014) Protein structure modeling with MODELLER. *Protein Structure Prediction*, 1-15
56. Phillips, J. C., Braun, R., Wang, W., Gumbart, J., Tajkhorshid, E., Villa, E., Chipot, C., Skeel, R. D., Kale, L., and Schulten, K. (2005) Scalable molecular dynamics with NAMD. *Journal of computational chemistry* 26, 1781-1802
57. Harvey, M. J., Giupponi, G., and Fabritiis, G. D. (2009) ACEMD: accelerating biomolecular dynamics in the microsecond time scale. *Journal of chemical theory and computation* 5, 1632-1639
58. Chodera, J. D., Swope, W. C., Pitera, J. W., and Dill, K. A. (2006) Long-Time Protein Folding Dynamics from Short-Time Molecular Dynamics Simulations. *Multiscale Model. Simul.* 5, 1214-1226
59. Prinz, J.-H., Wu, H., Sarich, M., Keller, B., Senne, M., Held, M., Chodera, J. D., Schütte, C., and Noé, F. (2011) Markov models of molecular kinetics: Generation and validation. *The Journal of chemical physics* 134, 174105
60. Pande, V. S., Beauchamp, K., and Bowman, G. R. (2010) Everything you wanted to know about Markov State Models but were afraid to ask. *Methods* 52, 99-105
61. Voelz, V. A., Bowman, G. R., Beauchamp, K., and Pande, V. S. (2010) Molecular simulation of ab initio protein folding for a millisecond folder NTL9 (1− 39). *Journal of the American Chemical Society* 132, 1526-1528
62. Beauchamp, K. A., McGibbon, R., Lin, Y. S., and Pande, V. S. (2012) Simple few-state models reveal hidden complexity in protein folding. *Proc Natl Acad Sci U S A* 109, 17807-17813
63. Lapidus, L. J., Acharya, S., Schwantes, C. R., Wu, L., Shukla, D., King, M., DeCamp, S. J., and Pande, V. S. (2014) Complex pathways in folding of protein G explored by simulation and experiment. *Biophysical journal* 107, 947-955
64. Voelz, V. A., Jäger, M., Yao, S., Chen, Y., Zhu, L., Waldauer, S. A., Bowman, G. R., Friedrichs, M., Bakajin, O., and Lapidus, L. J. (2012) Slow unfolded-state structuring in Acyl-CoA binding protein folding revealed by simulation and experiment. *Journal of the American Chemical Society* 134, 12565-12577
65. Kohlhoff, K. J., Shukla, D., Lawrenz, M., Bowman, G. R., Konerding, D. E., Belov, D., Altman, R. B., and Pande, V. S. (2014) Cloud-based simulations on Google Exacycle reveal ligand modulation of GPCR activation pathways. *Nat Chem* 6, 15-21
66. Adelman, J. L., Ghezzi, C., Bisignano, P., Loo, D. D., Choe, S., Abramson, J., Rosenberg, J. M., Wright, E. M., and Grabe, M. (2016) Stochastic steps in secondary active sugar transport. *Proceedings of the National Academy of Sciences* 113, E3960-E3966
67. Perez-Hernandez, G., Paul, F., Giorgino, T., De Fabritiis, G., and Noe, F. (2013) Identification of slow molecular order parameters for Markov model construction. *J Chem Phys* 139, 015102
68. Schwantes, C. R., and Pande, V. S. (2013) Improvements in Markov State Model Construction Reveal Many Non-Native Interactions in the Folding of NTL9. *J. Chem. Theory Comput.* 9, 2000-2009
69. Oja, E., and Hyvarinen, A. (2000) Independent component analysis: algorithms and applications. *Neural networks* 13, 411-430
70. Naritomi, Y., and Fuchigami, S. (2011) Slow dynamics in protein fluctuations revealed by time-structure based independent component analysis: The case of domain motions. *J. Chem. Phys.* 134, 065101
71. Beauchamp, K. A., Bowman, G. R., Lane, T. J., Maibaum, L., Haque, I. S., and Pande, V. S. (2011) MSMBuilder2: Modeling Conformational Dynamics at the Picosecond to Millisecond Scale. *J Chem Theory Comput* 7, 3412-3419

72. Harrigan, M. P., Sultan, M. M., Hernández, C. X., Husic, B. E., Eastman, P., Schwantes, C. R., Beauchamp, K. A., McGibbon, R. T., and Pande, V. S. (2017) MSMBuilder: Statistical Models for Biomolecular Dynamics. *Biophysical journal* 112, 10-15
73. Berezhkovskii, A., Hummer, G., and Szabo, A. (2009) Reactive flux and folding pathways in network models of coarse-grained protein dynamics. *J Chem Phys* 130, 205102
74. Kube, S., and Weber, M. (2007) A coarse graining method for the identification of transition rates between molecular conformations. *The Journal of chemical physics* 126, 024103
75. Deuflhard, P., and Weber, M. (2005) Robust Perron cluster analysis in conformation dynamics. *Linear algebra and its applications* 398, 161-184
76. Chodera, J. D., and Noé, F. (2014) Markov state models of biomolecular conformational dynamics. *Current Opinion in Structural Biology* 25, 135-144